



6

7

8

10

11

13

14

16

17

18

19

20

21

22

23

24

25

26 27

28

29

30

31

32

33

34

35

36

37

38

40

41

42

43

44

Article

Comprehensive optimization of the tripolar concentric ring electrode based on its finite dimensions model and confirmed by finite element method modeling

Oleksandr Makeyev 1,*, Yiyao Ye-Lin 2, Gema Prats-Boluda 2, and Javier Garcia-Casado 2

- ¹ School of STEM, Diné College, Tsaile, AZ 86556, USA; omakeyev@dinecollege.edu
- ² Centro de Investigación e Innovación en Bioingeniería, Universitat Politècnica de València, Valencia 46022, Spain; yiye@ci2b.upv.es (Y.Y.-L.); gprats@ci2b.upv.es (G.P.-B.); jgarciac@ci2b.upv.es (J.G.-C.)
- * Correspondence: omakeyev@dinecollege.edu; Tel.: +1-928-724-6960

Abstract: Optimization performed in this study is based on the finite dimensions model of the concentric ring electrode as opposed to the negligible dimensions model used in the past. This makes the optimization problem comprehensive since all of the electrode parameters including, for the first time, the radius of the central disc and individual widths of concentric rings are optimized simultaneously. The optimization criterion used is maximizing the accuracy of the surface Laplacian estimation since ability to estimate Laplacian at each electrode constitutes primary biomedical significance of concentric ring electrodes. For tripolar concentric ring electrodes, the optimal configuration was compared to previously proposed linearly increasing inter-ring distances and constant interring distances configurations of the same size and based on the same finite dimensions model. Obtained analytic results suggest that previously proposed configurations correspond to an almost two-fold and more than three-fold increases in Laplacian estimation error respectively compared to the optimal configuration proposed in this study. These analytic results are confirmed using finite element method modeling that was adapted to the finite dimensions model of the concentric ring electrode for the first time. Moreover, finite element method modeling results suggest that optimal electrode configuration may also offer improved sensitivity and spatial resolution.

Keywords: electrophysiology; measurement; wearable sensors; noninvasive; concentric ring electrodes; Laplacian; estimation; optimization; finite element method; modeling.

Citation: Lastname, F.; Lastname, F.; Lastname, F. Title. Sensors 2021, 21, x. https://doi.org/10.3390/xxxxx

Academic Editor: Firstname Lastname

Received: date Accepted: date Published: date

Publisher's Note: MDPI stays neutral with regard to jurisdictional claims in published maps and institutional affiliations.



Copyright: © 2021 by the authors. Submitted for possible open access publication under the terms and conditions of the Creative Commons Attribution (CC BY) license (https://creativecommons.org/licenses/by/4.0/).

1. Introduction

Concentric ring electrodes (CREs; tripolar configuration shown in Figure 1, panel A) are noninvasive electrodes for electrophysiological measurement with primary biomedical significance tied to their ability to accurately estimate the Laplacian (second spatial derivative of the surface potential) at each electrode which is not feasible with conventional disc electrodes (Figure 1, panel B). This ability entails enhanced spatial resolution and a better capability to differentiate the activity of dipole sources in different areas [1]. Properties shared by the majority of currently used CREs are: relatively small radius of the central disc (compared to the radius of the electrode) and/or equal and small widths of concentric rings (compared to the radius of the electrode) [2–12]. These properties stem, at least partially, from the use of the negligible dimensions model (NDM) of a CRE - a Cartesian grid where the central disc is represented by a single point (of negligible diameter) in the middle of the grid and rings are represented by concentric circles (of negligible width) around it. For example, since NDM was used to calculate Laplacian estimates for tripolar CRE (TCRE) in [13,14], it also influenced the design of respective physical electrodes. Previous results on improving the Laplacian estimation accuracy via CRE optimization were also based on NDM [15-17].

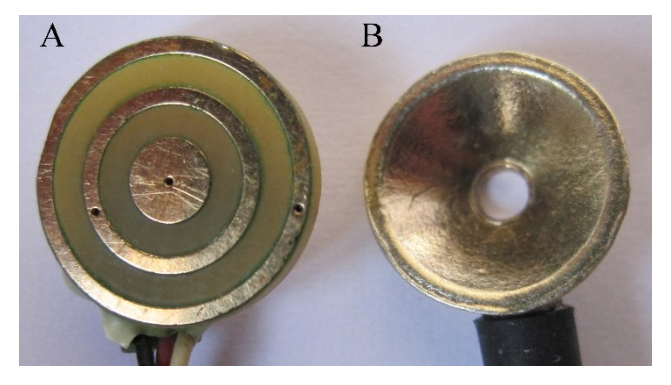


Figure 1. Tripolar concentric ring electrode (A) and conventional disc electrode (B).

First proof of concept of the finite dimensions model (FDM) of the CRE with nonnegligible individual widths of concentric rings and the radius of the central disc was introduced in [18] before being developed into a comparison framework validated on human electrocardiogram data in [7]. This framework, allowing direct comparison between two CRE configurations with the same number of rings and the same size but with different radii of the central disc, widths of concentric rings, and inter-ring distances, was used in this study to define and solve a comprehensive CRE optimization problem maximizing the accuracy of the Laplacian estimate signal recorded via said CRE. Unlike NDM based optimization problem that was solved in [17], this study includes and optimizes all the CRE parameters simultaneously. Absolute values of truncation term coefficients of the lowest remaining order were compared since in [16] and [17] ratios of those coefficients have been shown, using finite element method (FEM) modeling, to be predictors of the Laplacian estimation error. Specifically, ratios of Relative and Maximum Errors of Laplacian estimation calculated using FEM modeling and analytic ratios of truncation term coefficients differed by less than 5% for combinations of NDMs corresponding to linearly increasing inter-ring distances (LIIRD), constant inter-ring distances (CIRD), and linearly decreasing inter-ring distances (LDIRD) TCREs and quadripolar CREs [16] as well as for their quadratically increasing inter-ring distances counterparts [17]. Moreover, in [7] consistency between NDM and FDM in terms of values of truncation term coefficient ratios have been demonstrated for CIRD and LIIRD TCRE configurations. This is to be expected since NDM and FDM are also consistent in terms of the highest order of the truncation term that can be cancelled out during derivation of the Laplacian estimate that has been shown to be equal to twice the number of concentric rings in the electrode in [15] (for NDM) and [18] (for FDM) respectively.

As a result of the analytical portion of this study, general principles defining optimal CRE configurations maximizing the accuracy of Laplacian estimation are defined and illustrated for the case of TCREs. Moreover, optimal TCRE configuration is directly compared to LIIRD and CIRD configurations from [7]. CIRD configuration from [7] corresponds to a more than three-fold increase in Laplacian estimation error while LIIRD configuration from [7] corresponds to an almost two-fold increase in Laplacian estimation error compared to the optimal TCRE configuration proposed in this study. These analytic results are confirmed using FEM modeling via the NDM based FEM model from [13–17] that has been adapted to FDM for the first time. Moreover, FEM modeling results suggested that optimal electrode configuration may also offer improved sensitivity and spatial resolution compared to its counterparts.

2. Materials and Methods

2.1. Preliminaries

Figure 2 represents the FDM diagrams of three TCRE configurations including CIRD (Figure 2, panel A) and LIIRD (Figure 2, panel B) ones that were used to illustrate the

45 46

47

48

50

51

68

77

78

79 80 81

82

83

87

88

89

90

91

92

93

94

95

96

97

98

99

100

101

102

103

104

105

106

107

108

109

110

111

112

comparison framework in [7]. All three configurations in Figure 2 have the same radius subdivided into 9 equal intervals. CIRD and LIIRD configurations have the radius of the central disc and widths of both rings equal to 1/9 of the electrode radius. For CIRD configuration both distance between the central disc and the middle ring and distance between the middle ring and the outer ring are equal to 3/9 (= 1/3) of the electrode radius. For LIIRD configuration the distance between the central disc and the middle ring (2/9 of the electrode radius) is one half of the distance between the middle ring and the outer ring (4/9 of the electrode radius). Average potential on each concentric circle with the radius ranging from 1 to 9 is calculated using Huiskamp's Laplacian potential derivation based on the Taylor series expansion from [19]. Main steps of the comparison framework from [7] are listed below for TCRE configuration (see [7] for more detail on mathematical apparatus used for the analytical portion of this study) with similar steps used for quadripolar, pentapolar, etc configurations:

- Calculating the potentials on all three recording surfaces (central disc and two concentric rings) of the TCRE. For example, the potential on the central disc in all three TCRE configurations in Figure 2 is equal to the average of the potential at the center of the central disc and the potential on the concentric circle with radius equal to 1/9 of the electrode radius.
- 2. Canceling out the potential at the center of the central disc by taking bipolar differences between potentials on the middle ring and on the central disc and between potentials on the outer ring and on the central disc respectively.
- Combining the two bipolar differences linearly in order to cancel out the 4th (twice the number of concentric rings) order truncation term, to solve for the surface Laplacian estimate, and to calculate the absolute value of the 6th order truncation term coefficient (lowest remaining truncation term order for TCRE). Lowest remaining truncation term order is used since "higher-order terms usually contribute negligibly to the final sum and can be justifiably discarded" from the Taylor series [20].

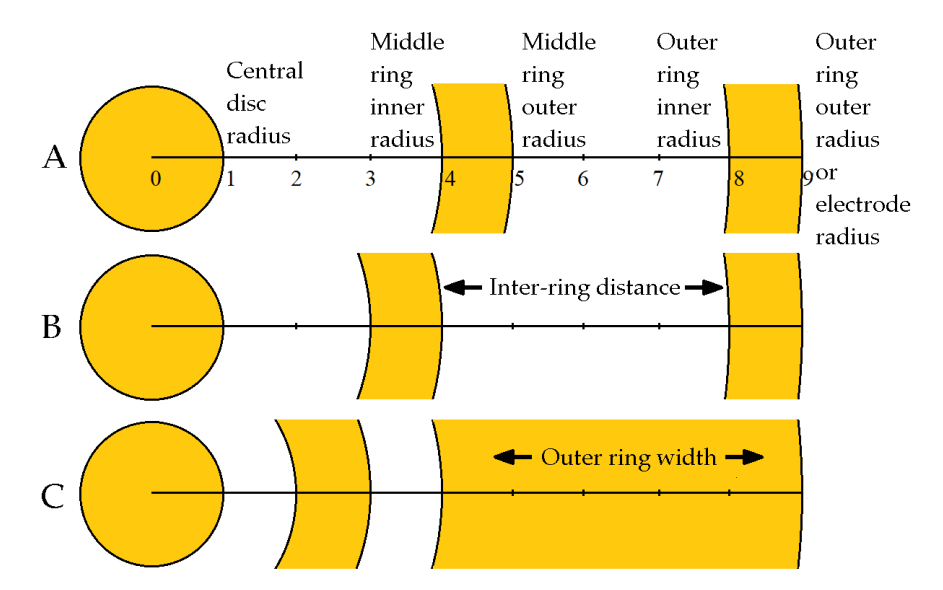


Figure 2. Finite dimensions models of three tripolar concentric ring electrode configurations including: (A) constant inter-ring distances configuration, (B) linearly increasing inter-ring distances configuration, and (C) optimal configuration with respect to the accuracy of Laplacian estimation.

2.2. Optimization Problem

Comparison framework from [7] has been developed into a comprehensive optimization problem directly comparing not pairs but all the possible CRE configurations of the same size and with the same number of rings simultaneously. Absolute values of truncation term coefficients for the lowest remaining truncation term order were calculated for

114

113

115

116

117

118 119 120

CRE configurations of given electrode size and with given number of rings including all the possible combinations of values for the radius of the central disc, widths of concentric rings, and inter-ring distances. The lowest absolute value of the truncation term coefficient corresponds to the highest accuracy of Laplacian estimation and vice versa. Optimization is illustrated for two scenarios, with the outer radius divided into 6 and into 9 equal intervals. The first case is a simpler scenario with a small number of possible combinations for disc and ring radii and widths that helps to identify the general principles that define optimal TCRE configurations. The second case allows to refine the search for the optimal configuration, to corroborate such general principles of optimization, and to directly compare the optimal TCRE configuration to previously proposed CIRD and LIIRD configurations.

2.3. FEM modeling

FEM model from [13–17] was adapted from NDM to FDM to directly compare the surface Laplacian estimates for CIRD and LIIRD TCRE configurations from [7] to the optimal (with respect to the accuracy of Laplacian estimation) TCRE configuration of the same size (Figure 2, panels A, B and C respectively). Matlab (Mathworks, Natick, MA, USA) was used for all the FEM modeling. An evenly spaced (0.278 mm) square mesh of 700×700 points corresponding to roughly 20×20 cm was located in the first quadrant of the *X-Y* plane over a unit charge dipole oriented towards the positive direction of the *Z* axis and projected to the center of the mesh (see Figure 3).

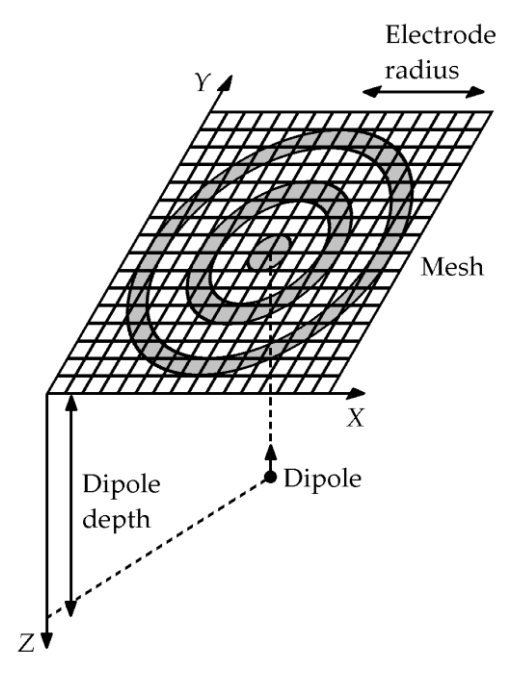


Figure 3. Schematic of the finite element method model used to compare Laplacian estimates.

Electric potential v was generated at each point of the mesh for different dipole depths ranging from 1 to 10 cm [21]:

$$v = \frac{1}{4\pi\sigma} \frac{(\overline{r}_p - \overline{r}) \cdot \overline{p}}{\left|\overline{r}_p - \overline{r}\right|^3} \tag{1}$$

where $\overline{r} = (x, y, z)$ is the location of the dipole, $\overline{p} = (p_x, p_y, p_z)$ is the moment of the dipole, and $\overline{r}_p = (x_p, y_p, z_p)$ is the observation point. The medium was assumed to be homogeneous with a conductivity σ equal to 7.14 mS/cm to emulate biological tissue [22].

The analytical Laplacian was calculated at each point of the mesh, by taking the second spatial derivative of the electric potential v [21]:

155

156

157

158

159

160

161

162

164

165

166

167

168

169

171172

173

174

175

176177

178

179

180

181

182 183

184185186

187

188 189

190

191

192

194

195

196

197

198

199

(4)

$$\nabla v = \frac{3}{4\pi\sigma} \left[5(z_p - z)^2 \frac{\left(\overline{r_p} - \overline{r}\right) \cdot \overline{p}}{\left|\overline{r_p} - \overline{r}\right|^7} - \frac{\left(\overline{r_p} - \overline{r}\right) \cdot \overline{p} + 2(z_p - z)p_z}{\left|\overline{r_p} - \overline{r}\right|^5} \right]$$
(2) 153

In order to obtain Laplacian estimates for the three TCRE configurations from Figure 2, potentials were calculated first for all nine concentric circles as means of potentials at four points on each circle. Next, these circle potentials were used to calculate the potentials on the three recording surfaces of each TCRE configuration. Finally, for each TCRE configuration, two bipolar differences for each of the ring potentials minus the central disc potential were linearly combined using respective set of coefficients and divided by the square of the distance between the concentric circles [7] to produce the respective Laplacian estimate. TCREs with outer diameters ranging from 0.5 cm to 5 cm were tested. Laplacian estimates were computed at each point of the mesh where appropriate boundary conditions could be applied for respective CRE diameter (the total number of points ranging from 520 x 520 for the largest CRE diameter to 682 x 682 for the smallest one). Laplacian estimate coefficients for the CIRD and LIIRD configurations (Figure 2, panels A and B) were adopted from [7]: (37/130, -11/468) for CIRD and (37/90, -7/540) for LIIRD respectively. Derivation of Laplacian estimate coefficients for the optimal configuration was performed using the analytic approach from [7] applied to the FDM from Figure 2, panel C and resulting in coefficients (952/1227, -6/409). These three Laplacian estimates were compared with the calculated analytical Laplacian for each point of the mesh, considering different dipole depths ranging from 1 cm to 10 cm, using the following measures:

Maximum Laplacian amplitude (Max(\nabla v)): Maximum amplitude of the analytical Laplacian as well as of the three Laplacian estimates corresponding to CIRD, LIIRD and optimal TCRE configurations in the mesh. It assesses the sensitivity to pick up the activity of the dipole.

Normalized spatial gradient (NSG): Assesses the change in the Laplacian potential with the displacement on the surface. The better the spatial resolution of the CRE, the more the NSG value should resemble that of the analytical. It is computed as the average of the normalized difference in the Laplacian potential from displacements at four cross-shaped points.

$$NSG(x_0, y_0, d) = \frac{1}{4} \left(\frac{|\nabla v(x_0, y_0) - \nabla v(x_0 - d, y_0)|}{\nabla v(x_0, y_0)} + \frac{|\nabla v(x_0, y_0) - \nabla v(x_0 + d, y_0)|}{\nabla v(x_0, y_0)} + \frac{|\nabla v(x_0, y_0) - \nabla v(x_0, y_0)|}{\nabla v(x_0, y_0)} + \frac{|\nabla v(x_0, y_0) - \nabla v(x_0, y_0 + d)|}{\nabla v(x_0, y_0)} \right)$$

$$(3)$$

where (x_0 , y_0) is the position where NSG is calculated (the center of the square mesh) and d is the distance equal to 0.5 cm (the smallest diameter of tested TCREs).

Relative (RE) and normalized maximum (NME) errors: RE assesses the total error and NME the normalized maximum error of the Laplacian estimate of TCRE over the whole mesh surface.

$$RE^{i} = \sqrt{\frac{\sum (\nabla v - \nabla^{i} v)^{2}}{\sum (\nabla v)^{2}}}$$
193

 $NME^{i} = \frac{\max|\nabla v - \nabla^{i}v|}{\max|\nabla v|} \tag{5}$

where i represents CRE configuration, $\nabla^i v$ represents the corresponding Laplacian estimate, and ∇v represents the analytical Laplacian. While (4) is borrowed verbatim from [13–17], (5) is a slight modification of the maximum error measure used in the aforementioned previous studies:

$$Maximum\ error^i = max |\nabla v - \nabla^i v|$$

(6)

The reason why the maximum error (6) from [13–17] was normalized in this study (5) was to make visualization of the improvement in Laplacian estimation accuracy easier by representing the error as a percentage of the maximum absolute value of the analytical Laplacian.

3. Results

3.1. General Principles Defining Optimal CRE Configurations

Before the general principles that define optimal CRE configurations maximizing the accuracy of Laplacian estimation are introduced, the results of optimization for TCRE with the outer radius of the outer ring (the electrode radius) equal to 6 are presented in Table 1. These results will be used to illustrate each of the aforementioned principles.

Table 1. All possible TCRE configurations for the outer radius of the outer ring equal to 6.

TCRE number	Central disc	Middle ring radii		Outer ring radii		Absolute value of the 6 th order	Increase with respect
	radius	Inner	Outer	Inner	Outer	truncation term	to the
						coefficient	optimal (%)
1	1	2	3	4	6	0.685	0
2	1	2	3	5	6	0.717	4.65
3	1	2	4	5	6	1.096	59.99
4	1	3	4	5	6	1.250	82.53
5	2	3	4	5	6	1.369	99.93

Table 1 contains all 5 possible TCRE configurations sorted in accordance with the respective absolute values of the 6th order truncation term coefficients whose ratios have been shown to be predictors of the Laplacian estimation error in [16,17] (hence the two terms are used interchangeably below). Percentage of increase in the absolute value of the 6th order truncation term coefficient with respect to the optimal configuration (TCRE configuration number 1) is also provided in the rightmost column of Table 1. It can be seen from Table 1 that even for such small electrode radius of 6 (reducing it further to 5 results in just a single possible TCRE configuration) the difference between the Laplacian estimation errors for the optimal and the worst-case scenario TCRE configurations (TCRE configuration number 5) approaches 100%.

General principles defining optimal CRE configurations in terms of accuracy of the surface Laplacian estimate are:

- 1. In the optimal configuration, central disc and concentric rings are kept at minimum distances with minimum radius/widths except for the width of the outer ring. Example: TCRE configuration number 1 in Table 1.
- 2. Larger width of the outer ring is advantageous to smaller width in electrode configurations that are otherwise identical. Example: TCRE configuration number 1 versus number 2 in Table 1.
- 3. Increasing the width of the outer ring of the electrode is advantageous to increasing the width of the middle ring. Example: TCRE configuration number 1 versus number 3 in Table 1.
- 4. Increasing the width of any concentric ring is advantageous to increasing the radius of the central disc. Example: TCRE configurations number 1 and 3 versus number 5 in Table 1.

5. Increasing the distance between recording surfaces closer to the outer edge is advantageous to increasing the distance between recording surfaces closer to the central disc. Example: TCRE configuration number 2 versus number 4 in Table 1.

3.2. Comparison of the Optimal TCRE Configuration with Previous Results

Table 2. Select TCRE configurations for the outer radius of the outer ring equal to 9.

			O		0 1		
TCRE number	Central disc	Middle ring radii		Outer ring radii		Absolute value of the 6 th order	Increase with respect
	radius	Inner	Outer	Inner	Outer	truncation term	to the
						coefficient	optimal (%)
1	1	2	3	4	9	1.447	0
2	1	2	3	5	9	1.458	0.78
3	1	2	3	6	9	1.489	2.94
4	1	2	3	7	9	1.550	7.19
5	1	2	3	8	9	1.650	14.07
				•••		•••	•••
15	1	3	4	8	9	2.883	99.33
						•••	•••
30	1	4	5	8	9	4.528	213.01
							•••
66	4	5	7	8	9	9.189	535.22
67	2	6	7	8	9	9.407	550.35
68	3	6	7	8	9	9.901	584.45
69	4	6	7	8	9	10.436	621.46
70	5	6	7	8	9	10.879	652.05

Out of the total of 70 possible TCRE configurations with radius equal to 9 Table 2 presents the top 5, the bottom 5, and two TCRE configurations assessed in [7]: CIRD (TCRE configuration number 30; Figure 2, panel A) and LIIRD (TCRE configuration number 15; Figure 2, panel B). While the results in Table 2 follow the same general principles defining optimal CRE configurations as the results in Table 1, the difference between the Laplacian estimation errors for the optimal and the worst-case scenario TCRE configurations increased to over 650% in Table 2 compared to under 100% in Table 1. This increase of more than 6.5 times is due to just 1.5 times increase in the electrode radius (from 6 in Table 1 to 9 in Table 2). More importantly, in direct comparison the optimal TCRE configuration (TCRE configuration number 1 in Table 2; Figure 2, panel C) outperforms LIIRD and CIRD configurations by 99.33% and 213.01% respectively in terms of the Laplacian estimation error.

3.3. FEM modeling

Maximum Laplacian amplitude, normalized spatial gradient and relative and normalized maximum errors computed via the FEM modeling are presented in Figure 4 for CRE diameters ranging from 0.5 cm to 5 cm and a dipole depth of 3 cm (as considered in [17]) for analytical, CIRD, LIIRD and optimal TCRE estimates.

Variation of the maximum amplitude of the Laplacian potential estimates with the electrode size is presented in panel A of Figure 4. For any electrode size, the optimal TCRE

provides the highest sensitivity since its amplitude values are the closest to those of analytical Laplacian, followed by the LIIRD and CIRD configurations respectively. The maximum amplitude for the analytical Laplacian corresponds to 0.825 mV/cm^2 . Differences between the maximum amplitudes of the analytical Laplacian and those of the CIRD, LIIRD and optimal estimates are minor for electrodes with an external diameter smaller than 1.5 cm. For larger TCRE sizes, sensitivity of estimates decreases, with a nonlinear drop being more or less pronounced depending on the Laplacian estimate (CIRD is the most affected TCRE configuration while the optimal TCRE is the least affected one). The lowest values of Max(∇v) correspond to the electrode with external diameter of 5 cm, with Max(∇v) of 0.76 mV/cm^2 , 0.78 mV/cm^2 , 0.80 mV/cm^2 for CIRD, LIIRD and optimal estimates respectively.

The NSG trend for a dipole depth of 3 cm with the increase in the electrode size is shown in panel B of Figure 4. Similarly to $Max(\nabla v)$, for an electrode diameter smaller than 1.5 cm, NSGs of the three Laplacian estimates are very similar to that of the analytical Laplacian (12.95 %). Furthermore, the greater the electrode diameter the greater the reduction in NSG for all Laplacian estimates with the optimal configuration being the one with the closest NSG values to the analytical Laplacian for all the electrode sizes, followed by the LIIRD and CIRD configurations. For the largest electrode size (5 cm in diameter) the NSG reduces to 12.3 %, 11.8 % and 11.4 % for optimal, LIIRD and CIRD Laplacian estimates respectively.

As for the RE and NME, depicted in panels C and D of Figure 4 respectively, the larger the electrode size the greater the error (both relative and normalized maximum) of the Laplacian estimates for all TCRE configurations (CIRD, LIIRD and optimal). Specifically, for the 5 cm external diameter relative and normalized maximum errors corresponding to CIRD configuration are equal to 5.65% and 8.31% respectively while optimal TCRE configuration allows decreasing them to 2.03% and 3.1%.

Figure 5 shows the evolution of the aforementioned measures computed via the FEM modeling for an electrode size of 3 cm and dipole depths ranging from 1 cm to 10 cm with logarithmic scale used in the vertical axis. $Max(\nabla v)$ (panel A) presents a nonlinear decrease as the dipole depth increases for analytical Laplacian and its three estimates, ranging from 5·10⁻² V/cm² (dipole at 1 cm) to 5·10⁻⁶ V/cm² (dipole at 10 cm). Greater changes in $Max(\nabla v)$ due to depth of the dipole mask the differences between the estimates via the three TCRE configurations (such as the ones observed in Figure 4, panel A), which are barely visible for dipoles deeper than 2 cm in panel A of Figure 5. As to NSG (panel B), differences between analytical Laplacian and its estimates are noticeable for dipoles at a depth of less than 3 cm, with a highest NSG at 1 cm of 70 % for the analytical Laplacian followed by estimates from optimal (65 %), LIIRD (60 %) and CIRD (58 %) configurations. NSG values drop nonlinearly with the dipole depth reaching 1.2 % at 10 cm. RE and NME (panels C and D respectively) also show a decreasing nonlinear trend as dipole depth increases. Estimates from CIRD entails the highest RE and NME for the entire range of depths tested followed by the LIIRD with the optimal configuration corresponding to the lowest errors. The most superficial dipole (1 cm) yields the largest errors: RE and NME of $25\,\%$ and $31\,\%$ for CIIRD, of 18% and $23\,\%$ for LIIRD and of $10\,\%$ and $14\,\%$, for the optimal configuration respectively.

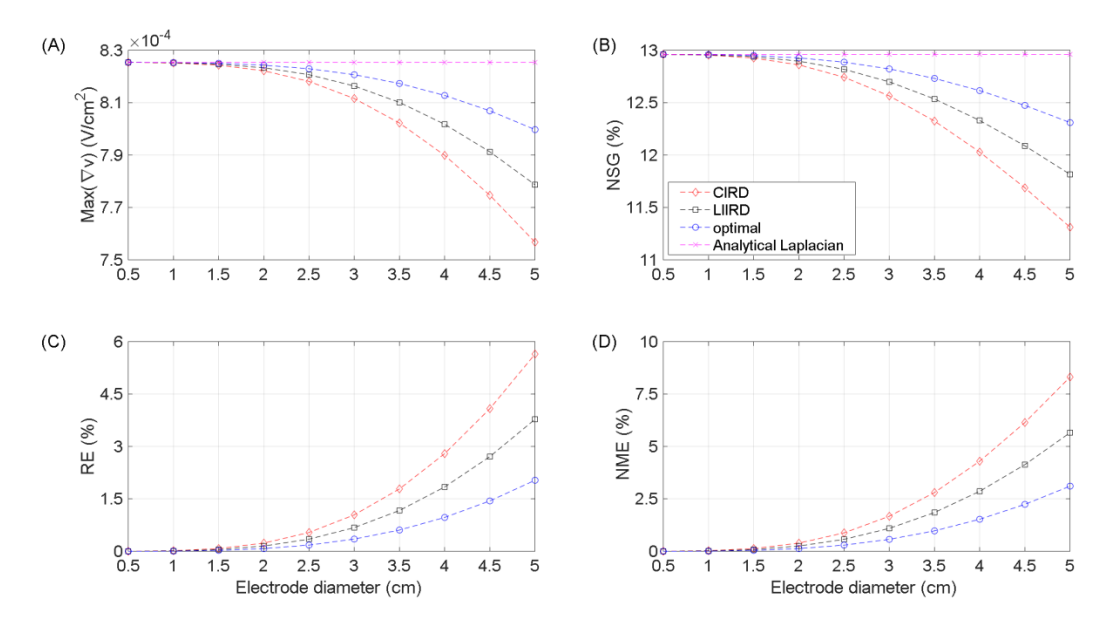


Figure 4. Maximum Laplacian amplitude $(Max(\nabla v))$, normalized spatial gradient (NSG), relative (RE) and normalized maximum errors (NME) computed via the finite element method modeling for tripolar concentric ring electrode diameters ranging from 0.5 cm to 5 cm and a dipole depth of 3 cm.

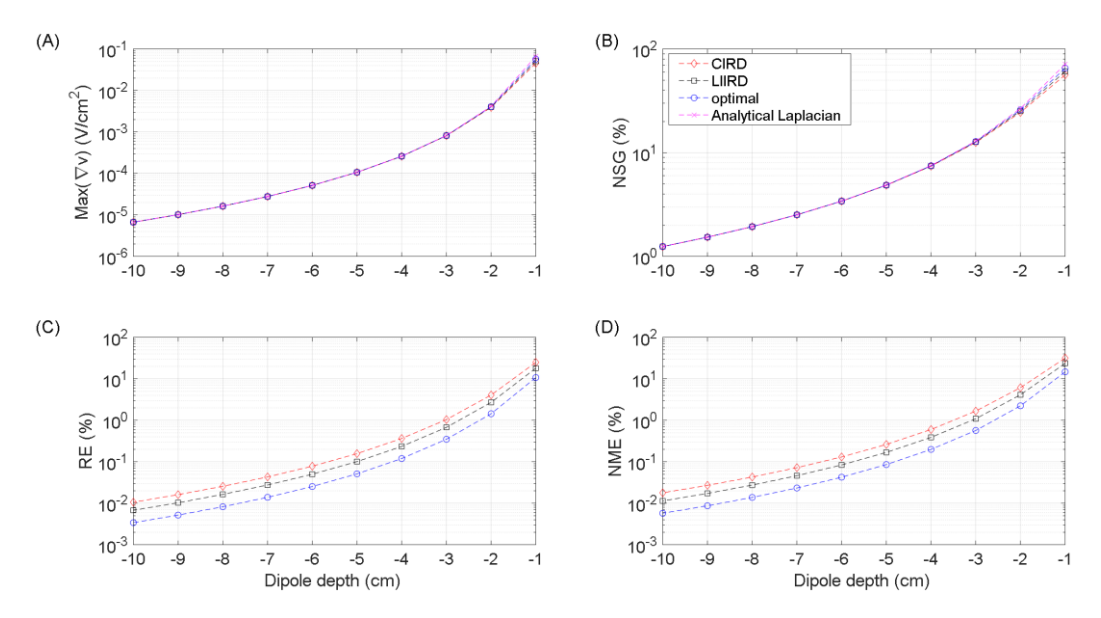


Figure 5. Maximum Laplacian amplitude (Max(∇v)), normalized spatial gradient (NSG), relative (RE) and normalized maximum errors (NME) computed via the finite element method modeling for a tripolar concentric ring electrode with diameter equal to 3 cm and dipole depths ranging from 1 cm to 10 cm.

For better comparison of the FEM results with analytical ones (shown in section 3.2), the increases in RE and NME with respect to the optimal configuration from CIRD and LIIRD were computed. Table 3 shows the mean \pm standard deviation of such increases (%) over the 10 CRE diameters studied for each dipole depth (ranging from 1 cm to 10 cm). It can be observed that the deeper the dipole the higher the mean values of increases in RE and NME but the lower their standard deviations. Moreover, increases of CIRD vs. optimal are higher than those of LIIRD vs. optimal for all dipole depths, with values at 1 cm of 143.3 \pm 42.8 % and 71.7 \pm 17.4 % respectively for increases in RE and of 129.6 \pm 48.7 % and 66.0 \pm 20.2 % respectively for increases in NME. At 10 cm depth, increases in RE reach

326

327

328

329

 211.4 ± 1.3 % and 98.7 ± 0.5 %, and increases in NME reach 211.0 ± 1.7 % and 98.6 ± 0.6 % for CIRD vs. optimal and LIIRD vs. optimal respectively.

Table 3. Mean and standard deviation of the increases (%) in relative (RE) and normalized maximum errors (NME) for constant inter-ring distances (CIRD) and linearly increasing inter-ring distances (LIIRD) tripolar concentric ring electrode (TCRE) configurations, compared to the optimal one, for electrode dimensions ranging from 0.5 cm to 5 cm at each dipole depth (ranging from 1 cm to 10 cm)

Dinala douth (am)	CIRD vs. op	timal TCRE	LIIRD vs. optimal TCRE		
Dipole depth (cm)	RE (%)	NME(%)	RE (%)	NME(%)	
1	143.3 ± 42.8	129.6 ± 48.7	71.7 ± 17.4	66.0 ± 20.2	
2	184.5 ± 21.0	176.7 ± 26.3	88.4 ± 8.1	85.4 ± 10.2	
3	198.2 ± 11.6	193.9 ± 14.9	93.7 ± 4.4	92.1 ± 5.7	
4	204.1 ± 7.2	201.4 ± 9.3	96.0 ± 2.7	95.0 ± 3.5	
5	207.1 ± 4.8	205.3 ± 6.3	97.1 ± 1.8	96.4 ± 2.4	
6	208.8 ± 3.5	207.6 ± 4.5	97.8 ± 1.3	97.3 ± 1.7	
7	209.9 ±2.6	209.0 ± 3.4	98.2 ± 1.0	97.8 ± 1.3	
8	210.6 ± 2.0	209.9 ± 2.6	98.4 ± 0.8	98.2 ± 1.0	
9	211.1 ± 1.6	210.5 ± 2.1	98.6 ± 0.6	98.4 ± 0.8	
10	211.4 ± 1.3	211.0 ± 1.7	98.7 ± 0.5	98.6 ± 0.6	

4. Discussion

In this study, optimization of the FDM based TCRE configuration with respect to the accuracy of Laplacian estimation is performed. The distinctive feature of obtained results (Tables 1 and 2) is that in optimal TCRE configurations the recording surfaces account for the vast majority of the electrode surface area via minimizing the distances between the recording surfaces (e.g. optimal TCRE configuration in Figure 2, panel C). This is markedly different from the currently used CREs where majority of the electrode surface area corresponds to the distances between the recording surfaces (for example, CREs from [7,8] or TCRE from panel A of Figure 1). Compared to the optimal TCRE configuration (Figure 2, panel C), LIIRD configuration of the same size (Figure 2, panel B) increases the Laplacian estimation error almost two-fold while CIRD configuration (Figure 2, panel A) corresponds to a more than three-fold increase. Analytic and FEM based increases in Laplacian estimation error are shown to be consistent (difference of less than 5%): medians of mean FEM modeling-based increases in Laplacian estimation error from Table 3 are equal to 97.45% and 96.85% (RE and NME respectively) as well as to 207.95% and 206.45% (RE and NME respectively) which is comparable to increases of 99.33% and 213.01% obtained analytically (Table 2).

General increase in the surface Laplacian estimation errors due to increase in the electrode size (Figure 4, panels C and D) is consistent with the previously obtained results via NDM based FEM modeling [13–17] and demonstrated for the first time in this study via FDM based FEM modeling. Another aspect of FDM based optimal configurations that is consistent with the previous results obtained using NDM is locating the middle ring closer to the central disc than to the outer ring which is consistent with analytical and FEM modeling results from [16,17].

Increasing the electrode size also leads to a greater deviation of NSG values corresponding to TCRE Laplacian estimates with respect to that of analytical Laplacian. It is well known that the larger the electrode size the poorer the spatial resolution and selec-

332

333

334

> > 358

359

348

349

361

362

363

364

365

367

368

369

370

371

372

373

374

375

376

377

378

379

380

381

382

383

384

385

386

387

388

389

390

391

392

393

394

395

396

397

399

400

401

402

403

404

406

407

408

409

410

411

412

413

tivity [23,24,4], nonetheless the CRE configuration also affects this. Optimal TCRE configuration provided the closest NSG values to that of analytical Laplacian and can partially 'compensate' for the effect of the electrode size. For example, optimal TCRE configuration of 5 cm in diameter yielded similar results to those of LIIRD of 4 cm diameter and CIRD of 3.5 cm diameter for dipole depth at 3 cm (Figure 4, panel B). It may seem weird that maximum amplitudes of Laplacian estimates decrease for larger electrode sizes (Figure 4, panel A) when reported amplitudes of signals recorded with CRE are greater for larger electrodes [25,24,4]. However, it has to be taken into consideration that while units of Laplacian signal are mV/cm², those of recorded potential are mV, and they are related through the square of the electrode diameter. Therefore, despite this small decrease in the Laplacian amplitude obtained for larger electrode sizes in the FEM results (Figure 4, panel A), the amplitude of the raw potential signals to be recorded under experimental conditions can be expected to increase with an increase in the electrode size. In fact, in various applications [11,12] it has been seen that lower amplitude of the signals captured with CREs compared to signals recorded via conventional disc electrodes can lead to signals of poorer quality (lower signal-to-noise ratio) therefore suggesting the need to use larger CREs while having to sacrifice the spatial resolution. In this sense, the optimal TCRE configuration has been shown to provide the highest Laplacian amplitude values for a given electrode size (Figure 4, panel A), thus offering a quantitative advantage over other TCRE configurations such as CIRD or LIIRD.

Regarding the influence of the dipole depth, as it could be expected, the closer is the dipole to the body surface the greater the amplitude (Figure 5, panel A) and the gradient (Figure 5, panel B) of the Laplacian potential. It can also be observed (Figure 5, panels C and D) that the errors of Laplacian estimation are greater for closer dipoles. In this context, the two- and three-fold reduction in estimation errors obtained for the optimal TCRE configuration in comparison to LIIRD and CIRD ones are more meaningful for smaller dipole depths and could be significant in real life noninvasive electrophysiological measurement applications.

The only optimization criterion used in this study was maximizing the accuracy of surface Laplacian estimation via the CRE. Other optimization criteria may result in different optimal electrode configurations so adding additional criteria to the optimization problem solved in this study is one of the potential directions of the future work. More importantly, for optimal CRE configurations the question of how small can the distances between the recording surfaces get before shorting due to salt bridges negatively affects the accuracy of Laplacian estimation becomes more critical than before since the first principle defining optimal configurations is to keep those distances minimal. Prototyping of the optimal TCRE configuration is needed to answer this question. Therefore, future work will concentrate on building prototypes of optimal adhoc designed TCREs comparing them against LIIRD and CIRD configurations as well as against conventional single pole (e.g. conventional disc) electrodes on real life data recordings including phantom, animal model and human for further proof. Future work also involves moving from a single-layer FEM model used in this study to a more comprehensive one such as, for example, a fivelayer planar model of the abdomen [26] or a four-layer concentric inhomogeneous spherical head model used recently in [10]. Finally, the issue of flexibility of the electrode substrate and its possible effect on the accuracy of the Laplacian estimation merits further investigation since both analytical and FEM modeling studies carried out to date have always considered CRE on a plane and placing a flexible CRE on a curved body surface may partially change its response. Although so far performance of flexible real life CREs has been consistent with the results of analytical studies [2,7,8] the effect of increase in body surface curvature has not been studied.

Results obtained in this study are important since they have potential to influence the design of future CREs and could not have been obtained with simplistic NDM. Confirmation of analytic results using FEM modeling further suggests the potential of the optimal TCRE configuration proposed in this study in particular as well as the potential of

415

416

417

418

419

420

421

422

423

424

425

426

427

428

430

431

432

433

434

435

436

437

438

439

440

441

442

443 444

446

447

448

449

450

451

452

453

454

455

456

457

458

459

460 461

462

463

464

the FDM based comprehensive optimization of the CRE design targeting maximizing the accuracy of the surface Laplacian estimation in general. Moreover, FEM modeling has been used to illustrate the promise of the optimal TCRE configuration with respect to improved sensitivity and spatial resolution as well as to investigate the effect of the dipole depth. To illustrate how insights stemming from this study can be incorporated into the design of future CREs for real-life applications the following example can be considered. Shortly after LDIRD and LIIRD CRE configurations were first introduced and compared to their CIRD counterparts in [16], stencil printed TCRE prototypes closely resembling (and explicitly referencing [16]) LIIRD configuration were assessed on human electroencephalogram, electrocardiogram, and electromyogram data with obtained results suggesting enhanced spatial resolution and localization of signal sources [2]. Those results were obtained despite of the physical TCRE prototypes from [2] having a 1:3 ratio of inter-ring distances compared to the 1:2 ratio proposed in [16]. To the best of our knowledge, physical prototypes of variable inter-ring distances TCREs from [2] were the first ones and they stemmed from the analytical and FEM modeling results obtained in [16]. Next, bipolar, tripolar (LDIRD and LIIRD) and quadripolar (CIRD) CREs were compared to standard 12-lead recordings on human electrocardiogram data from twenty volunteers [8]. Not only did the obtained results show that normalized amplitude of the P-wave of signals recorded via CRE at CMV1 was significantly greater than any of the standard 12-lead recordings offering better contrast for the study of the P-wave important in practical diagnostic applications but that the relationship between different CRE configurations in terms of their normalized amplitude of the P-wave and signal-to-noise ratio was consistent with analytical results for Laplacian estimation error from [16] (for two tripolar configurations assessed) and [15] (for bipolar versus tripolar versus quadripolar configurations). Other examples of recent biomedical applications of CREs that could potentially benefit from the insights stemming from this study include but are not limited to electroencephalogram (source localization of high-frequency activity [6] and seizure detection [9] in epilepsy patients), electroenterogram (identification of the intestinal slow waves [3]) and electromyogram (evaluation of swallowing [11] and respiratory [12] muscle activity) based ones.

5. Patents

Patent number 11,045,132 "Concentric ring electrodes for improved accuracy of Laplacian estimation" resulting from the work reported in this manuscript has been issued by the United States Patent and Trademark Office on June 29th, 2021.

Author Contributions: Conceptualization, O.M. and J.G.-C.; methodology, O.M., Y.Y.-L., G.P.-B., and J.G.-C.; software, O.M. and Y.Y.-L.; validation, O.M., Y.Y.-L., G.P.-B., and J.G.-C.; formal analysis, O.M.; writing—original draft preparation, O.M., G.P.-B., and J.G.-C.; writing—review and editing, O.M., Y.Y.-L., G.P.-B., and J.G.-C.; visualization, Y.Y.-L.; supervision, J.G.-C.; funding acquisition, O.M. All authors have read and agreed to the published version of the manuscript.

Funding: This research was funded by the National Science Foundation (NSF) Division of Human Resource Development (HRD) Tribal Colleges and Universities Program (TCUP), grant number 1914787 to O.M.

Data Availability Statement: The data presented in this study are available on request from the corresponding author.

Acknowledgments: O.M. gratefully acknowledges Dr. Ernst Kussul and Dr. Tetyana Baydyk (National Autonomous University of Mexico, Mexico) for the constructive discussions and helpful comments.

Conflicts of Interest: The authors declare no conflict of interest. The funders had no role in the design of the study; in the collection, analyses, or interpretation of data; in the writing of the manuscript, or in the decision to publish the results.

References 465

1. Besio, W.G.; Chen, T. Tripolar Laplacian Electrocardiogram and Moment of Activation Isochronal Mapping. *Physiological measurement* **2007**, *28*, 515, doi:10.1088/0967-3334/28/5/006.

- 2. Wang, K.; Parekh, U.; Pailla, T.; Garudadri, H.; Gilja, V.; Ng, T.N. Stretchable Dry Electrodes with Concentric Ring Geometry for Enhancing Spatial Resolution in Electrophysiology. *Adv Healthc Mater* **2017**, *6*, doi:10.1002/adhm.201700552.
- 3. Zena-Giménez, V.; Garcia-Casado, J.; Ye-Lin, Y.; Garcia-Breijo, E.; Prats-Boluda, G. A Flexible Multiring Concentric Electrode for Non-Invasive Identification of Intestinal Slow Waves. *Sensors* **2018**, *18*, 396.
- 4. Prats-Boluda, G.; Ye-Lin, Y.; Pradas-Novella, F.; Garcia-Breijo, E.; Garcia-Casado, J. Textile Concentric Ring Electrodes: Influence of Position and Electrode Size on Cardiac Activity Monitoring. *Journal of Sensors* **2018**, 2018, e7290867, doi:https://doi.org/10.1155/2018/7290867.
- 5. Nasrollaholhosseini, S.H.; Mercier, J.; Fischer, G.; Besio, W. Electrode-Electrolyte Interface Modeling and Impedance Characterizing of Tripolar Concentric Ring Electrode. *IEEE Trans Biomed Eng* **2019**, doi:10.1109/TBME.2019.2897935.
- 6. Toole, C.; Martinez-Juárez, I.E.; Gaitanis, J.N.; Sunderam, S.; Ding, L.; DiCecco, J.; Besio, W.G. Source Localization of High-Frequency Activity in Tripolar Electroencephalography of Patients with Epilepsy. *Epilepsy Behav* **2019**, *101*, 106519, doi:10.1016/j.yebeh.2019.106519.
- 7. Makeyev, O.; Musngi, M.; Moore, L.; Ye-Lin, Y.; Prats-Boluda, G.; Garcia-Casado, J. Validating the Comparison Framework for the Finite Dimensions Model of Concentric Ring Electrodes Using Human Electrocardiogram Data. *Applied Sciences* **2019**, 9, 4279, doi:10.3390/app9204279.
- 8. Garcia-Casado, J.; Ye-Lin, Y.; Prats-Boluda, G.; Makeyev, O. Evaluation of Bipolar, Tripolar, and Quadripolar Laplacian Estimates of Electrocardiogram via Concentric Ring Electrodes. *Sensors* **2019**, *19*, 3780, doi:10.3390/s19173780.
- 9. Aghaei-Lasboo, A.; Inoyama, K.; Fogarty, A.S.; Kuo, J.; Meador, K.J.; Walter, J.J.; Le, S.T.; Graber, K.D.; Razavi, B.; Fisher, R.S. Tripolar Concentric EEG Electrodes Reduce Noise. *Clinical Neurophysiology* **2020**, *131*, 193–198.
- 10. Liu, X.; Makeyev, O.; Besio, W. Improved Spatial Resolution of Electroencephalogram Using Tripolar Concentric Ring Electrode Sensors. *Journal of Sensors* **2020**, 2020, 6269394, doi:10.1155/2020/6269394.
- 11. Garcia-Casado, J.; Prats-Boluda, G.; Ye-Lin, Y.; Restrepo-Agudelo, S.; Perez-Giraldo, E.; Orozco-Duque, A. Evaluation of Swallowing Related Muscle Activity by Means of Concentric Ring Electrodes. *Sensors* **2020**, *20*, 5267, doi:10.3390/s20185267.
- 12. Estrada-Petrocelli, L.; Torres, A.; Sarlabous, L.; Ràfols-de-Urquía, M.; Ye-Lin, Y.; Prats-Boluda, G.; Jané, R.; Garcia-Casado, J. Evaluation of Respiratory Muscle Activity by Means of Concentric Ring Electrodes. *IEEE Transactions on Biomedical Engineering* **2021**, *68*, 1005–1014, doi:10.1109/TBME.2020.3012385.
- 13. Besio, W.G.; Koka, K.; Aakula, R.; Dai, W. Tri-Polar Concentric Ring Electrode Development for Laplacian Electroencephalography. *IEEE Transactions on Biomedical Engineering* **2006**, *53*, 926–933.
- 14. Besio, W.G.; Aakula, R.; Koka, K.; Dai, W. Development of a Tri-Polar Concentric Ring Electrode for Acquiring Accurate Laplacian Body Surface Potentials. *Ann Biomed Eng* **2006**, *34*, 426–435, doi:10.1007/s10439-005-9054-8.
- 15. Makeyev, O.; Ding, Q.; Besio, W.G. Improving the Accuracy of Laplacian Estimation with Novel Multipolar Concentric Ring Electrodes. *Measurement* **2016**, *80*, 44–52, doi:10.1016/j.measurement.2015.11.017.
- 16. Makeyev, O.; Besio, W.G. Improving the Accuracy of Laplacian Estimation with Novel Variable Inter-Ring Distances Concentric Ring Electrodes. *Sensors* **2016**, *16*, 858, doi:10.3390/s16060858.
- 17. Makeyev, O. Solving the General Inter-Ring Distances Optimization Problem for Concentric Ring Electrodes to Improve Laplacian Estimation. *BioMedical Engineering OnLine* **2018**, *17*, 117, doi:10.1186/s12938-018-0549-6.
- 18. Makeyev, O.; Lee, C.; Besio, W.G. Proof of Concept Laplacian Estimate Derived for Noninvasive Tripolar Concentric Ring Electrode with Incorporated Radius of the Central Disc and the Widths of the Concentric Rings. *Conf Proc IEEE Eng Med Biol Soc* 2017, 2017, 841–844, doi:10.1109/EMBC.2017.8036955.

19.	Huiskamp, G. Difference Formulas for the Surface Laplacian on a Triangulated Surface. Journal of Computational Physics 1991,	507
	95, 477–496, doi:10.1016/0021-9991(91)90286-T.	508
20.	King, M.R.; Mody, N.A. Numerical and Statistical Methods for Bioengineering: Applications in MATLAB; Cambridge University	509
	Press, 2010;	510
21.	He, B.; Wu, D. Laplacian Electrocardiography. Crit Rev Biomed Eng 1998, 27, 285-338.	511
22.	Besio, W.G.; Fasiuddin, M. Quantizing the Depth of Bioelectrical Sources for Non-Invasive 3D Imaging. J Bioelectromagn 2005,	512
	7, 90–3.	513

- 23. Kaufer, M.; Rasquinha, L.; Tarjan, P. Optimization of Multi-Ring Sensing Electrode Set. In Proceedings of the Proceedings of the Annual Conference on Engineering in Medicine and Biology; Publ by IEEE, December 1 1990; pp. 612–613.
- 24. Ye-Lin, Y.; Bueno-Barrachina, J.M.; Prats-boluda, G.; Rodriguez de Sanabria, R.; Garcia-Casado, J. Wireless Sensor Node for Non-Invasive High Precision Electrocardiographic Signal Acquisition Based on a Multi-Ring Electrode. *Measurement* 2017, 97, 195–202, doi:10.1016/j.measurement.2016.11.009.
- 25. Ye-Lin, Y.; Alberola-Rubio, J.; Prats-boluda, G.; Perales, A.; Desantes, D.; Garcia-Casado, J. Feasibility and Analysis of Bipolar Concentric Recording of Electrohysterogram with Flexible Active Electrode. *Ann Biomed Eng* **2014**, 43, 968–976, doi:10.1007/s10439-014-1130-5.
- 26. Garcia-Casado, J.; Zena, V.; Perez, J.J.; Prats-Boluda, G.; Ye-Lin, Y.; Garcia-Breijo, E. Opened-Ring Electrode Array for Enhanced Non-Invasive Monitoring of Bioelectrical Signals: Application to Surface EEnG Recording. In Proceedings of the Biomedical Engineering Systems and Technologies; Fernández-Chimeno, M., Fernandes, P.L., Alvarez, S., Stacey, D., Solé-Casals, J., Fred, A., Gamboa, H., Eds.; Springer: Berlin, Heidelberg, 2014; pp. 26–40.